Electronic Supplementary Material (ESI) for Environmental Science: Water Research & Technology.

Influence of colloidal iron oxide and natural organic matter (NOM) fouling on nanofiltration (NF) membrane performance: role of feed composition and membrane properties

Supporting Information

Desislava Filipova Davidkova[1], Margaret Graham[2], Santiago Romero-Vargas Castrillón[1,3*], Andrea Joana Correia Semião[1*]

[1] Institute for Infrastructure and Environment, School of Engineering, The University of Edinburgh, William Rankine Building, Thomas Bayes Road, Edinburgh EH9 3FG United Kingdom

[2] School of Geosciences, The University of Edinburgh, Crew Building, Alexander Crum Brown Road, Edinburgh EH9 3FF, United Kingdom

[3] Institute for Materials and Processes, School of Engineering, The University of Edinburgh, Sanderson Building, Robert Stevenson Road, Edinburgh EH9 3FB United Kingdom

[*] authors to whom correspondence should be addressed:

E-mail address: Andrea.Semiao@ed.ac.uk

E-mail address: Santiago@ed.ac.uk

Supporting methods and materials

S.1. Iron oxide colloidal stability

Stability experiments carried out with the synthesised iron oxide colloids confirmed the findings from previous studies about the dependence of particle size on solution pH, ionic strength and TOC concentration [1,2]. High pH (> pH 6), high ionic strength (I > 10 mM) and/or low NOM concentration (5 – 10 mg C/L) caused the formation of macroscopic aggregates that underwent gravitational settling within 24 hours (data not shown). These results can be explained by the iso-electric point of iron oxides being around circum-neutral pH, and reduction in electrostatic repulsion due to charge screening and neutralisation of positive surface charges by negatively-charged organic matter, respectively. In contrast, at pH 5.5 and I = 1 mM, experiments up to 72 hours in duration confirmed that there was no significant particle size growth or settling for solutions containing 40 mg/L Fe oxide (with or without 20 mg/L SRNOM) in the presence of monovalent salt (NaCl) or divalent salt ($CaCl_2$) (Fig. S1). Ultimately, pH 5.5 and I = 1 mM were chosen for the membrane filtration experiments.

S.2. Membrane characterisation protocols

Contact angle: The hydrophobicity of the SBNF and NF270 membranes was quantified by contact angle measurements, using the sessile drop method. Membrane coupons were attached to a glass slide using double-sided tape and dried in a desiccator overnight. UP water droplets (2 μL) were deposited on the membrane coupons in a goniometer (DSA30, Kruss) equipped with a temperature controlled chamber ($T = 20 \pm 0.5$ °C). The right-hand-side and left-hand-side contact angles of 4 droplets per membrane type were recorded using the ADVANCE software for image analysis, for a total of 8 measurements per membrane. The effect of deposition time was investigated, with a comparison of the droplet contact angle at $t = 0$ s and $t = 20$ s. The contact angle was found to be independent of deposition time (Fig. S3).

Surface zeta potential: The surface zeta potential (ζ) of the pristine membranes was measured using an electrokinetic analyser (SurPASSIII, Anton Paar, Austria) in a 1 mM KCl background electrolyte solution. The pH of the solution was adjusted with NaOH (0.1 mM) and HCl (0.1 mM) solutions. Measurements were done in duplicate for each membrane over the pH range 2.6 – 8.

Surface roughness: The surface morphology and roughness of the pristine membranes was determined by tapping-mode atomic force microscopy (AFM). Scans were collected using an AFM (JPK NanoWizard 4XP, Bruker) equipped with a fluid cell filled with NaCl or $CaCl_2$ background electrolyte solution of the same compositions as used the fouling experiments ($I = 1$ mM, pH = 5.5, $T = 20$ °C). Three 5×5-μm^2 scans were obtained for each membrane in each solution at a scan rate of 0.25 Hz using an SNL-10 probe (cantilever "C", Bruker). Images were processed using the Gwyddion software, which also allowed the calculation of the root-mean-square roughness (R_{RMS}) of 5 random 1×1-μm^2 sections samples from each AFM image.

Cryo-SEM-EDX sample preparation and analysis: Surface and cross-section morphology, along with elemental analysis of the pristine and fouled membranes, were studied using scanning electron microscopy (Crossbeam 550 FIB-SEM, Zeiss) and energy-dispersive X-ray spectroscopy (XMax^N 150 detector, Oxford Instruments) (SEM-EDX). The SEM-EDX was equipped with cryogenic attachment

(PP3010T, Quorum Technologies) that facilitated SEM micrographs of the membranes in hydrated state. Pristine and fouled membrane samples for the SEM-EDX analysis were kept in ultrapure (UP) water (18.2 MΩ cm) to ensure that the morphology of the membranes was not altered due to dehydration. Immediately before imaging, the samples were removed from solution, cut and glued (using equal parts of colloidal graphite (G303, Aquadag®) and OCT compound (Scigen®)) onto a copper stub. The samples were dipped in slushed nitrogen, sublimed for 5 minutes ($T = -90$ °C, $p \approx 10^{-7}$ mbar) and sputter coated with platinum or chromium to ensure high conductivity of the sample. During the imaging the probe current used was 50 – 100 pA and the acceleration voltage was 5 – 20 kV.

S.3. Calculation of electrostatic double-layer (F_{EDL}) interaction force

The electrostatic double layer interaction force (F_{EDL}) was calculated for particle-particle interactions (e.g., assuming an existing layer of particles on the membrane), using the measured average particle size and zeta potential (Fig. S1) for the following fouling scenarios: Fe oxide + SRNOM + $CaCl_2$ and Fe oxide + SRNOM +NaCl. The theory by Derjaguin, Landau, Verwey and Overbeek (DLVO) states that the EDL repulsive force between two spherical particles is given by [3]:

$$F_{EDL} = \frac{\pi D \lambda \sigma^2}{\varepsilon \varepsilon_0} \exp\left(\frac{-h_c}{\lambda}\right)$$

where F_{EDL} is the electrostatic force [N]; D is the particle diameter [m]; λ is the Debye length [m] (equal to 9.6×10^{-9} m for $I = 1$ mM); $\sigma = \frac{\varepsilon \varepsilon_0 \zeta}{\lambda}$ is the charge density [C m^{-2}]; ζ is particle surface (zeta) potential [J C^{-1}]; ε_0 is the permittivity in free space [8.854×10^{-12} C^2 J^{-1} m^{-1}]; ε is the dielectric constant of the solvent ($\varepsilon = 80$ for water); h_c is the critical separation distance of maximum barrier force [m] (which is assumed to be 0.158×10^{-9} m based on other studies [4]). The Debye length is calculated from [3]:

$$\lambda = \left(\frac{\varepsilon \varepsilon_0 k_B T}{e^2 \sum_i z_i^2 \rho_{i,\infty}}\right)^{0.5}$$

where k_B is the Boltzmann constant [J K^{-1}]; T is the absolute temperature [293.15 K]; e is the elementary charge [1.6×10^{-19} C]; z_i is the charge of ionic species i; $\rho_{i,\infty}$ is the bulk number concentration of the ionic species i [m^{-3}]. The values of $\rho_{i,\infty}$ and z_i for the different solution chemistries are specified in Table A:

Table A. Parameters used to calculate the Debye length (λ) for 1 mM NaCl and 0.3 mM CaCl2 solution (total ionic strength I = 1 mM); $\rho_{i,\infty}$ is calculated by multiplying the molar concentration by Avogadro's number (6.022×10^{23})

Solution	Chemical species, *i*	Charge, z_i	Molar concentration [mM]	Bulk number concentration, $\rho_{i,\infty}$ [number of atoms m^{-3}]
1 mM NaCl	Na	+1	1	6.02×10^{23}
	Cl	-1	1	6.02×10^{23}
0.33 mM $CaCl_2$	Ca	+2	0.33	2.01×10^{23}
	Cl	-1	0.67	4.01×10^{23}

The results, shown in Table B, show that a reduction in the particle surface potential from |-33| mV to |-18| mV leads to a threefold decrease in F_{EDL}.

Table B. Experimentally determined colloid diameter (D), zeta potential (ζ), calculated charge density (σ) and electrostatic double-layer interaction force (F_{EDL}).

System	$D \times 10^{-9}$ [m]	$\zeta \times 10^{-3}$ [J C^{-1}]	$\sigma \times 10^{-9}$ [C m^{-2}]	$F_{EDL} \times 10^{-11}$ [N]
Fe oxide + SRNOM + $CaCl_2$	59.79	-17.90	-1.32	0.44
Fe oxide + SRNOM + NaCl	55.10	-33.05	-2.44	1.37

Supporting results

Table S1. TOC concentration of two SRNOM stock solutions (2 g/L) measured over time to assess any change in stock TOC content during long-term storage. The values show the mean of 3 replicate measurements ± standard deviation.

	TOC concentration [g/L]		
Stock #	Day 1	Day 15	Day 56
1	773.4 ± 3.0	753.6 ± 4.25	
2	751.3 ± 7.4		762.3 ± 2.7

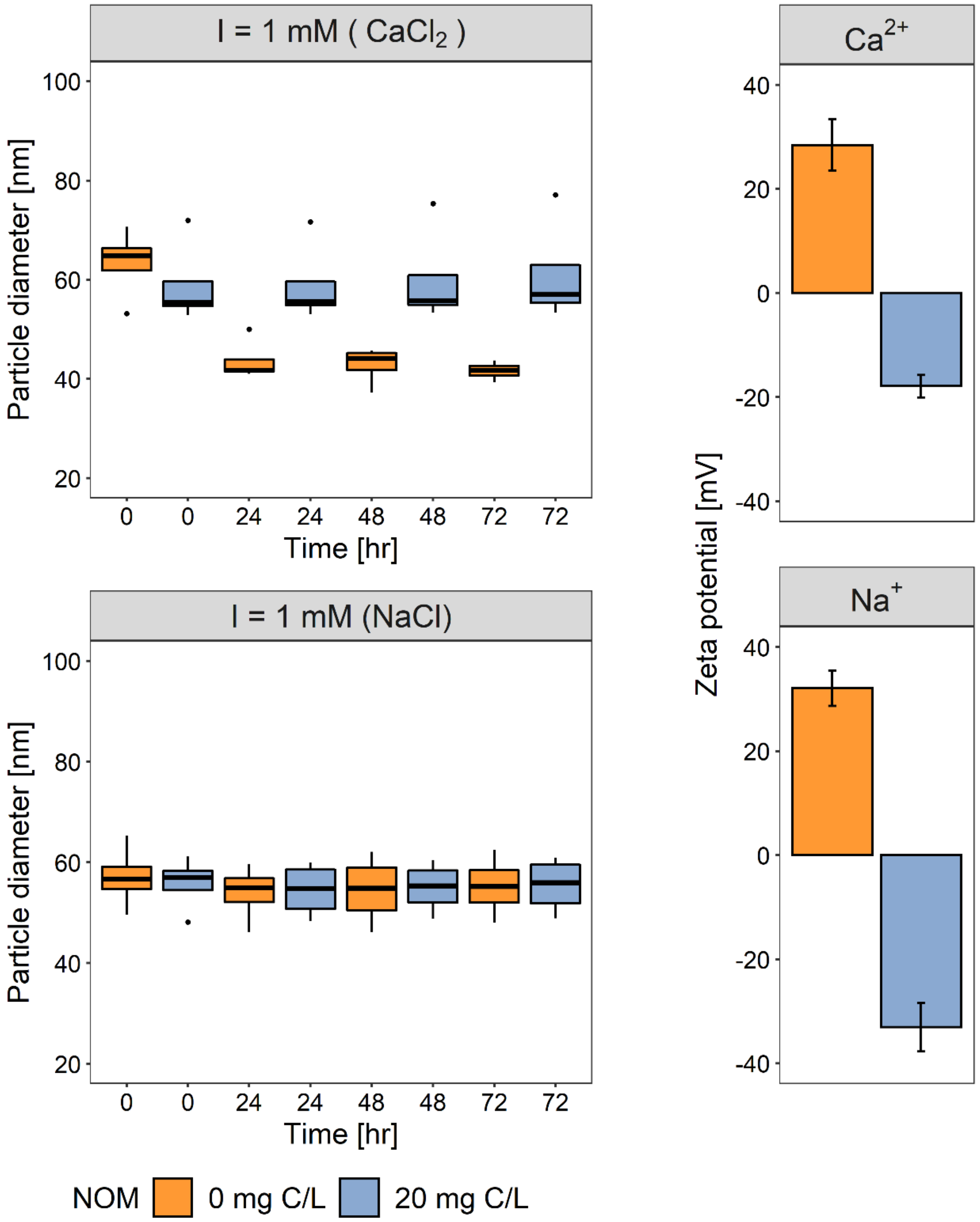

Figure S1. Time dependence of iron oxide (40 mg/L) particle size and zeta potential in the presence and absence of SRNOM (0 – 20 mg C/L) in CaCl$_2$ solution (top) or NaCl solution (bottom). All data shown are at pH = 5.5 and ionic strength *I* = 1 mM. Boxplots show median, 25th percentile and 75th percentile; whiskers show maximum and minimum values; dots indicate outliers. For bar charts, error bars indicate standard deviation of measurements from *n* = 4 replicates.

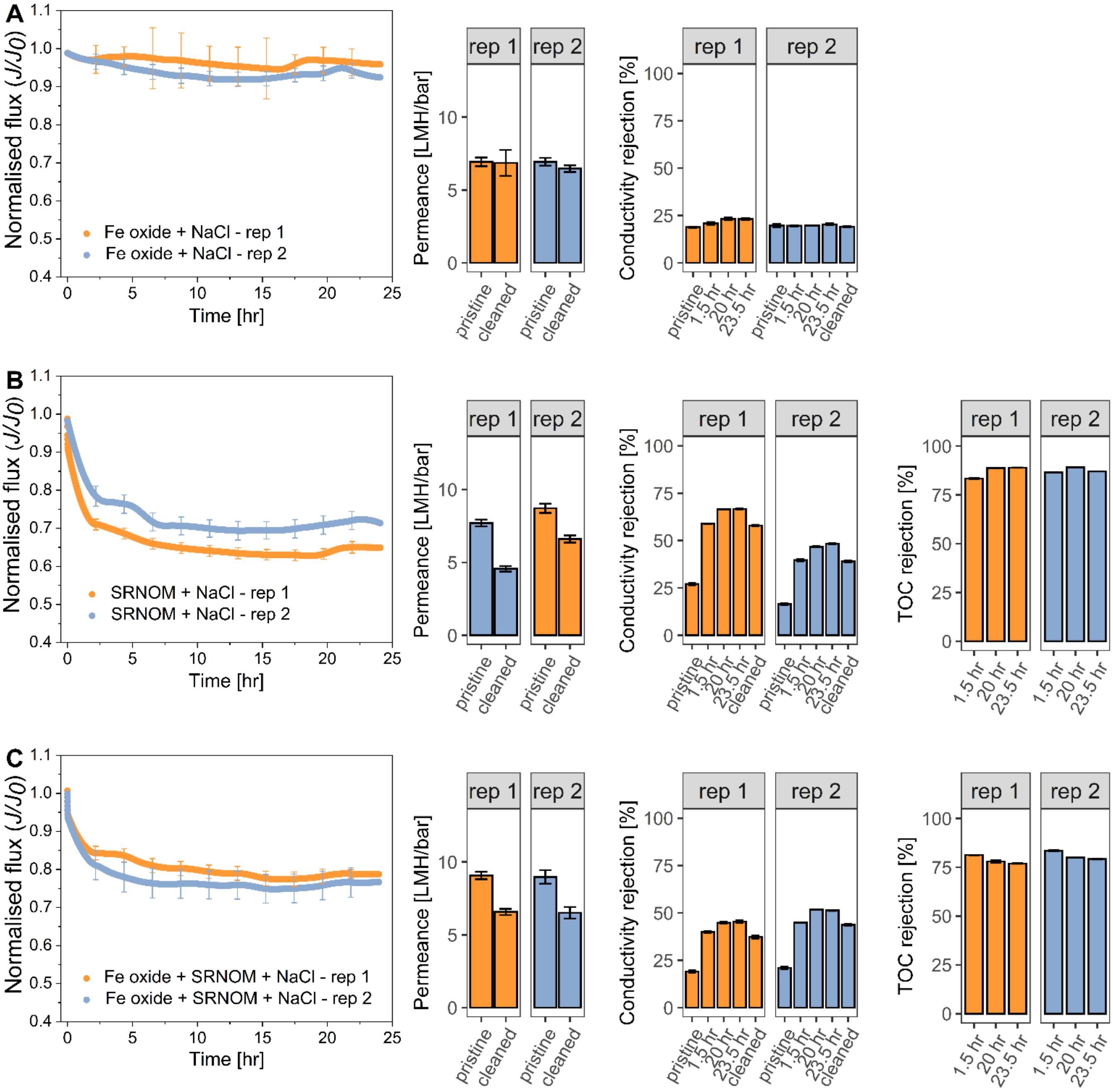

Figure S2. Normalised flux (J/J_0) over time from individual replicate experiments (orange and blue) with monovalent salt (NaCl) for each type of foulant: A. Fe oxide (40 mg /L); B. SRNOM (20 mg C/L); C. Fe oxide (40 mg/L) + SRNOM (20 mg C/L). Fouling conditions: cellulose acetate (SBNF) membrane, temperature (T = 20 °C), crossflow rate (u = 0.23 m/s, Re = 450), initial flux (J_0 = 100 LMH), pH = 5.5 and ionic strength (I = 1 mM). Flux data were smoothed using the loess function (span = 0.2) and the error bars show standard deviation. Error bars on the bar graphs indicate standard deviation from 3 measurements.

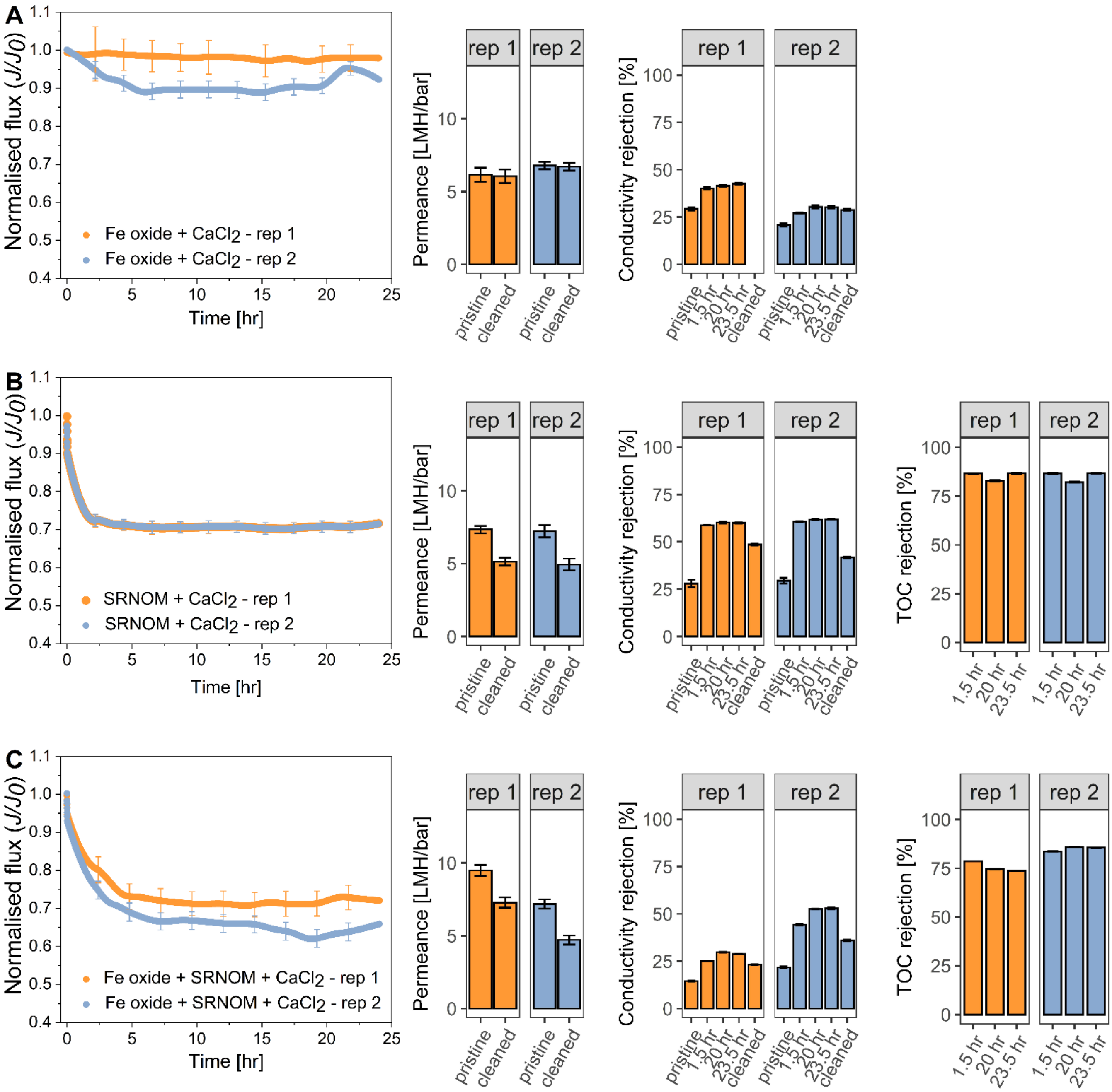

Figure S3. Normalised flux (J/J_0) over time from individual replicate experiments (orange and blue) with divalent salt ($CaCl_2$) for each type of foulant: A. Fe oxide (40 mg/L); B. SRNOM (20 mg C/L); C. Fe oxide (40 mg/L) + SRNOM (20 mg C/L). Fouling conditions: cellulose acetate (SBNF) membrane, temperature (T = 20 °C), crossflow rate (u = 0.23 m/s, Re = 450), initial flux (J_0 = 100 LMH), pH = 5.5 and ionic strength (I = 1 mM). Flux data were smoothed using the loess function (span = 0.2) and the error bars show standard deviation. Error bars on the bar graphs indicate standard deviation from 3 measurements.

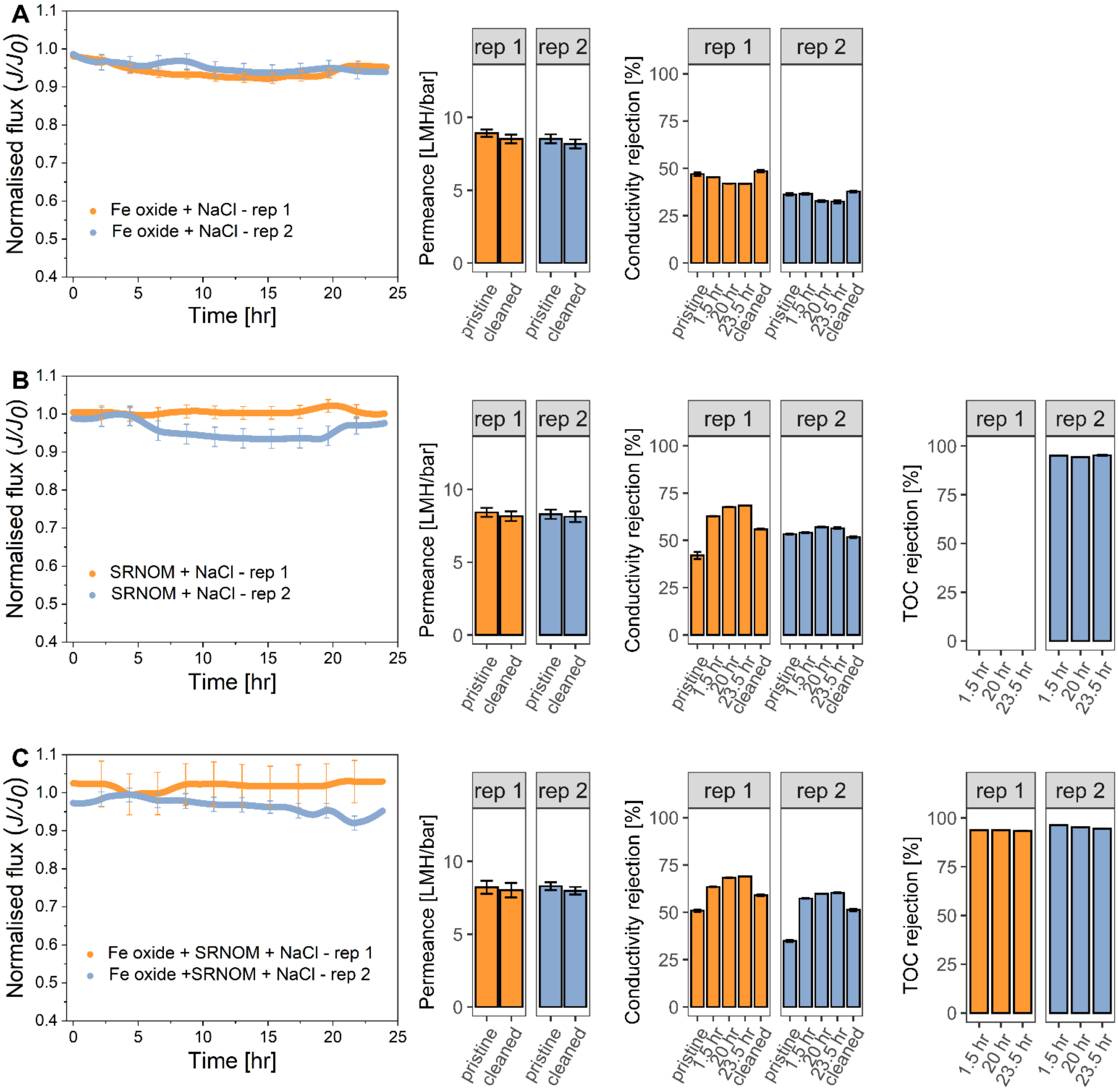

Figure S4. Normalised flux (J/J_0) over time from individual replicate experiments (orange and blue) with monovalent salt (NaCl) for each type of foulant: A. Fe oxide (40 mg/L); B. SRNOM (20 mg C/L); C. Fe oxide (40 mg/L) + SRNOM (20 mg C/L). Fouling conditions: polypiperazine amide (NF270) membrane, temperature (T = 20 °C), crossflow rate (u = 0.23 m/s, Re = 450), initial flux (J_0 = 100 LMH), pH = 5.5 and ionic strength (I = 1 mM). Flux data were smoothed using the loess function (span = 0.2) and the error bars show standard deviation. Error bars on the bar graphs indicate standard deviation from 3 measurements.

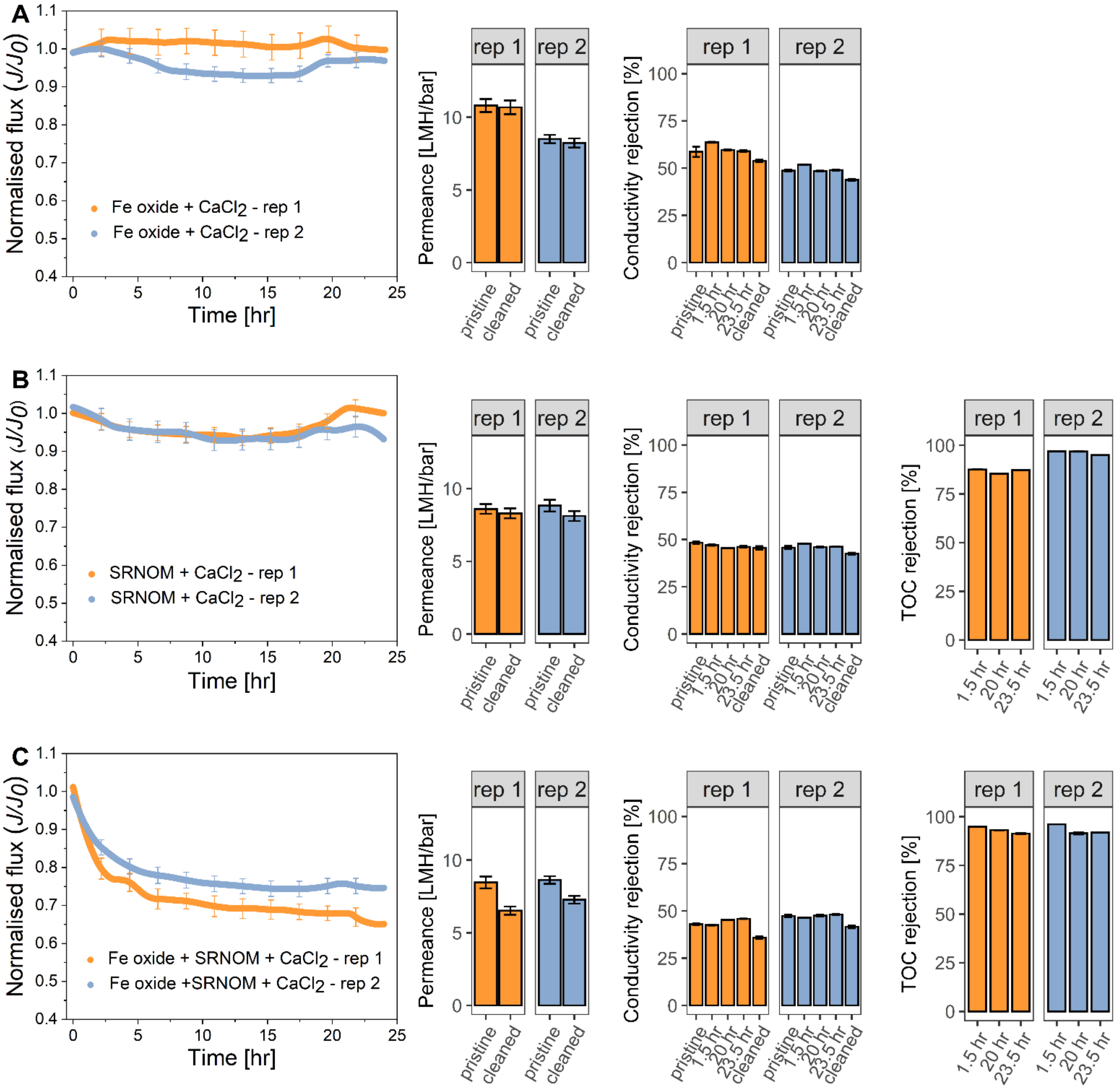

Figure S5. Normalised flux (J/J_0) over time from individual replicate experiments (orange and blue) with divalent salt ($CaCl_2$) for each type of foulant: A. Fe oxide (40 mg/L); B. SRNOM (20 mg C/L); C. Fe oxide (40 mg/L) + SRNOM (20 mg C/L). Fouling conditions: polypiperazine amide (NF270) membrane, temperature (T = 20 °C), crossflow rate (u = 0.23 m/s, Re = 450), initial flux (J_0 = 100 LMH), pH = 5.5 and ionic strength (I = 1 mM). Flux data were smoothed using the loess function (span = 0.2) and the error bars show standard deviation. Error bars on the bar graphs indicate standard deviation from 3 measurements.

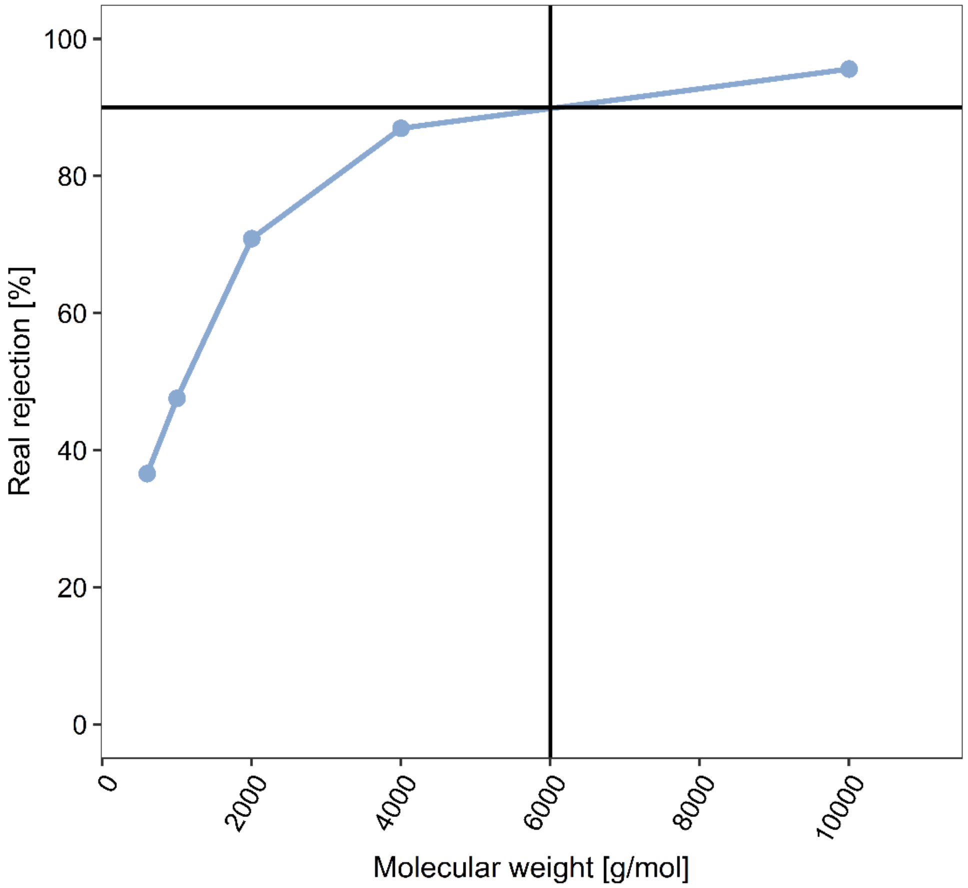

Figure S6. Real rejection of polyethylene glycol (PEG) of different molecular weight (600 – 10,000 Da) by SBNF cellulose acetate membranes. The rejection was determined at constant pressure *TMP* = 4 bar, *J* = 38.2 ± 1.3 LMH, *T* = 20 °C, *u* = 1.33 m/s (*Re* = 2564). Horizontal black line indicates 90 % rejection.

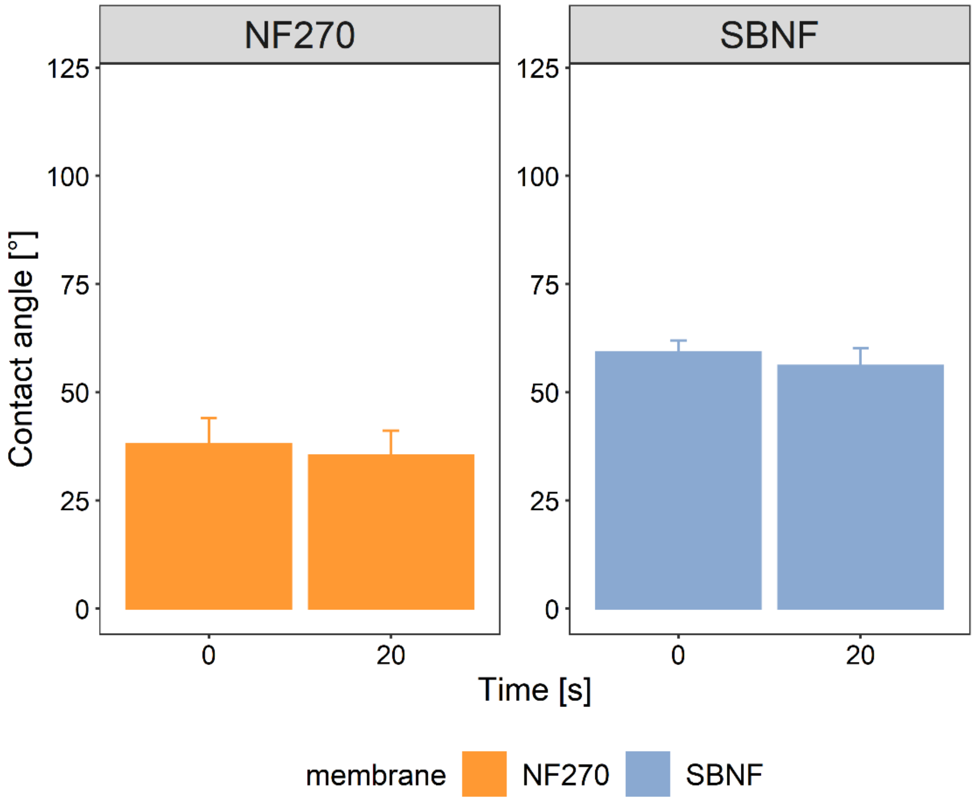

membrane	Time [s]	Contact angle [°]	st dev	N
NF270	0	38.0	6.1	8
NF270	20	35.4	5.8	8
SBNF	0	59.2	2.7	8
SBNF	20	56.1	4.1	8

Figure S7. Contact angle measurements at t = 0 s and t = 20 s of NF270 and SBNF membranes. Measurements were obtained using the sessile drop method. The table shows average values, standard deviation and number of replicates (N).

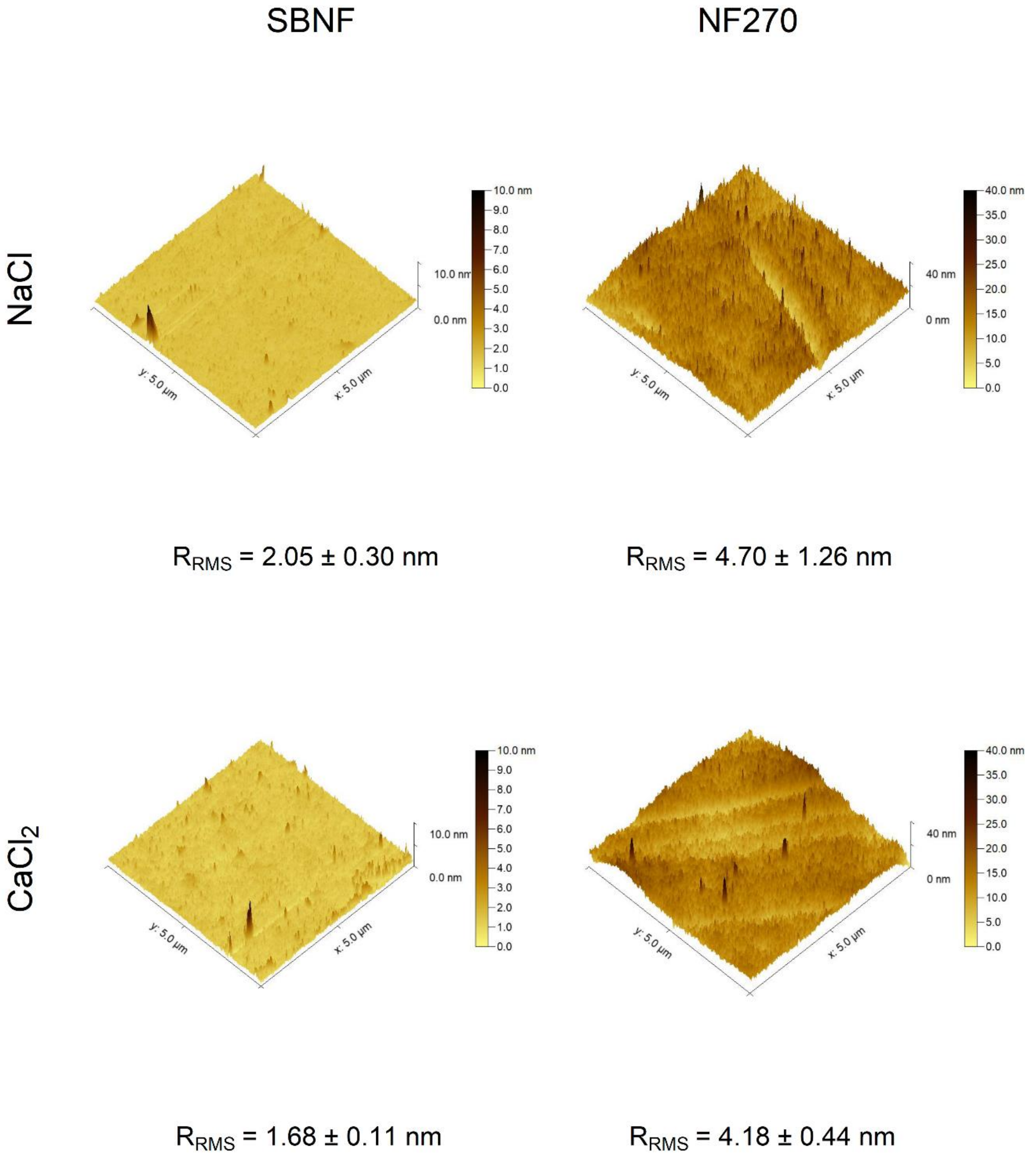

Figure S8. AFM surface images of pristine SBNF (left) and NF270 (right) membranes determined in NaCl (top) or $CaCl_2$ (bottom) solution. I = 1 mM, pH = 5.5. RMS roughness values below each image indicate an average and standard deviation of five 1-μm^2 random sections sampled within each of the images shown.

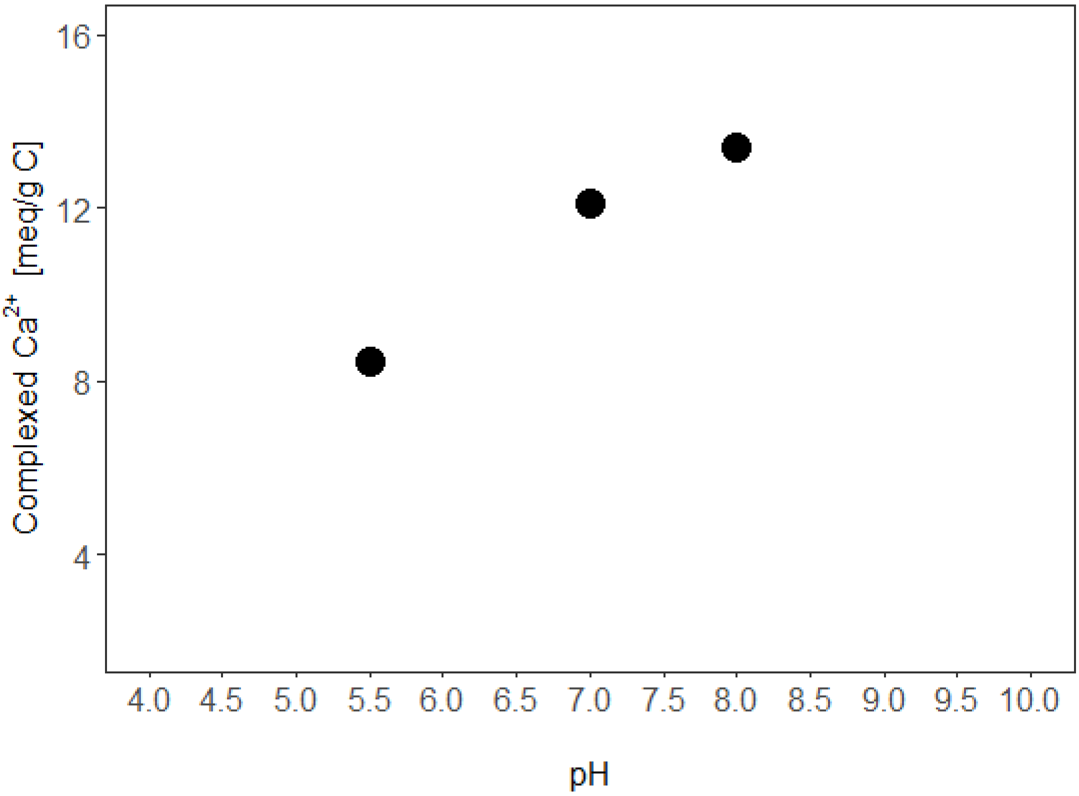

Figure S9. Complexation of Ca^{2+} by NOM as a function of solution pH. Concentration of SRNOM is 20 mg C/L and the solution total $CaCl_2$ is 0.334 mM (I = 1 mM). Complexed calcium is determined by the difference between the total calcium and measured free calcium in solution, and expressed per weight of organic carbon

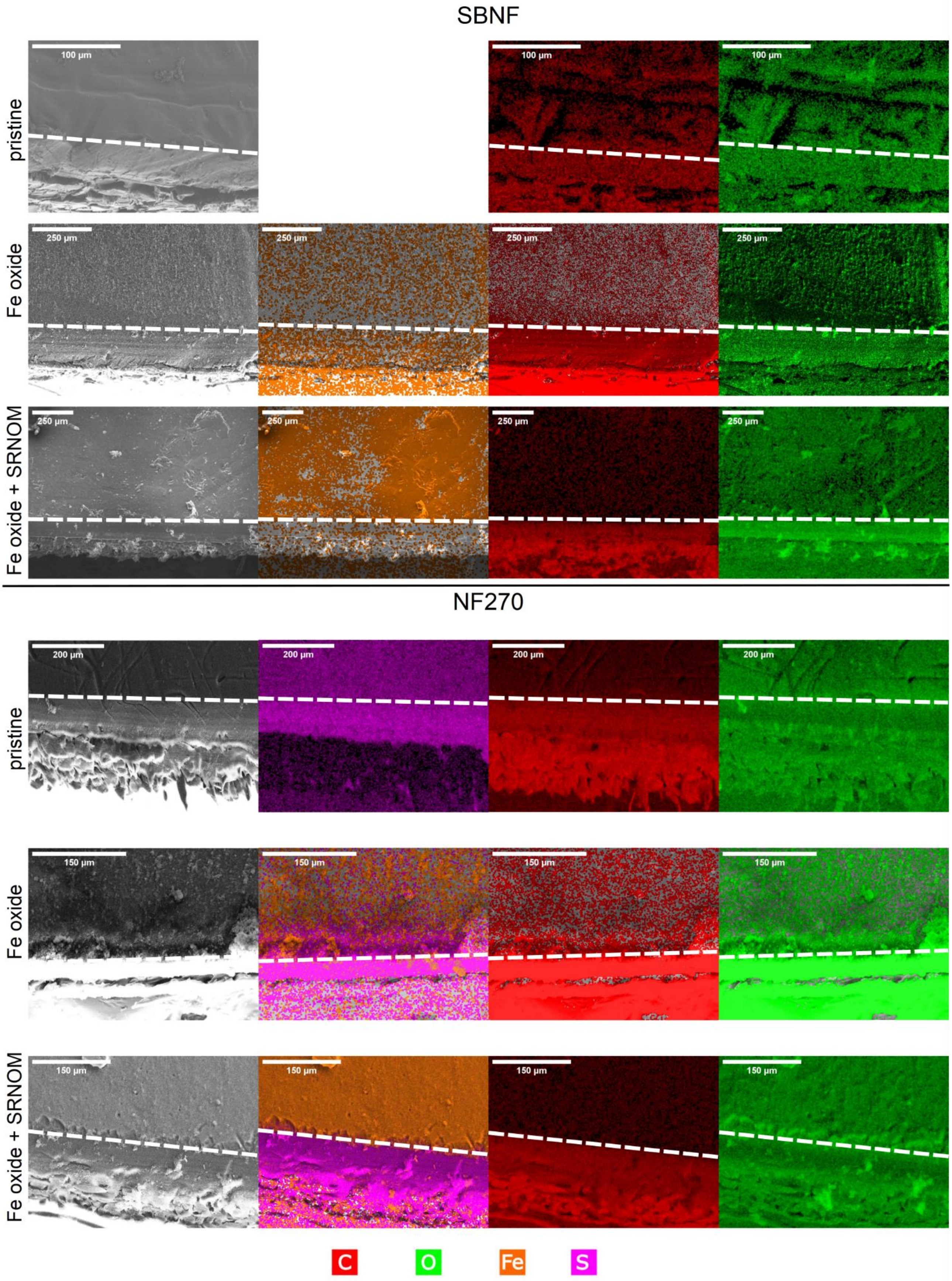

Figure S10. SEM micrographs and EDX-generated elemental maps of pristine and fouled membranes with Fe oxide or Fe oxide + SRNOM for SBNF (top) and NF270 (bottom) membranes. Images show the cross-section and active layer surface of the membranes (tilted at 30° – 60°). The white dashed line indicates the approximate location of the foulant-active layer interface. (C – carbon, O – oxygen, Fe – iron, S – sulphur).

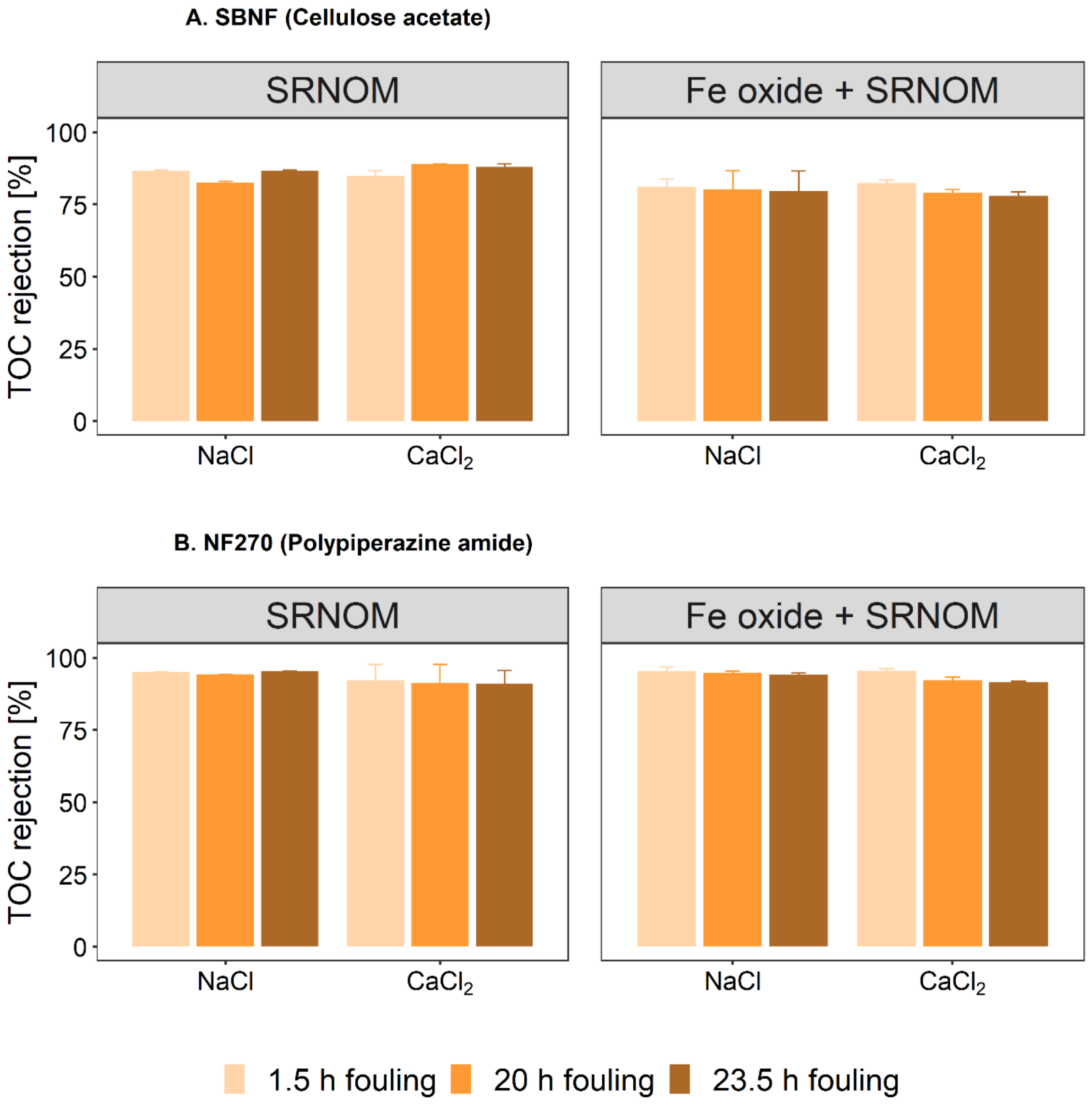

Figure S11. Total organic carbon (TOC) rejection during fouling (1.5 hr, 20 hr and 23.5 hr) of cellulose acetate (SBNF) (A) and polypiperazine amide (NF270) (B) membranes during organic (20 mg C/L SRNOM) and mixed (40 mg/L Fe oxide + 20 mg C/L) fouling experiments. Fouling conditions: temperature (T = 20 °C), crossflow rate (u = 0.23 m/s, Re = 450), initial flux (J_0 = 100 LMH), pH = 5.5 and ionic strength (I = 1 mM). Error bars indicate standard deviation of measurements from two replicate experiments.

References:

1. Gilbert B, Lu G, Kim CS. Stable cluster formation in aqueous suspensions of iron oxyhydroxide nanoparticles. J Colloid Interface Sci. 2007 Sep 1;313(1):152–9.

2. Hu JD, Zevi Y, Kou XM, Xiao J, Wang XJ, Jin Y. Effect of dissolved organic matter on the stability of magnetite nanoparticles under different pH and ionic strength conditions. Sci Total Environ. 2010 Jul 15;408(16):3477–89.

3. Israelachvili J. Intermolecular and Surface Forces. 3rd ed. Intermolecular and Surface Forces. Elsevier Inc.; 2011.

4. Tang CY, Kwon YN, Leckie JO. The role of foulant-foulant electrostatic interaction on limiting flux for RO and NF membranes during humic acid fouling-Theoretical basis, experimental evidence, and AFM interaction force measurement. J Memb Sci. 2009 Jan 20;326(2):526–32.